Efficiency Mapping and Weighted Average Efficiency for Large Hydrogenerators

EDSON DA COSTA BORTONI [ID] [1] **(Senior Member, IEEE),**
ROBERTO TEIXEIRA SINISCALCHI [ID][2] **(Senior Member, IEEE), SILVIO VASCHETTO**[3] **(Senior Member, IEEE),**
MOSTAFA AHMADI DARMANI [ID][3] **(Student Member, IEEE), AND ANDREA CAVAGNINO** [ID][3] **(Fellow, IEEE)**

[1]Itajubá Federal University, Electric and Energy Systems Institute, Itajubá, MG 37500-050, Brazil
[2]Furnas Centrais Eletricas, Minas Production Department, São José da Barra, MG 37945-000, Brazil
[3]Politecnico di Torino, Dipartimento di Energia, 10129 Turin, Italy

CORRESPONDING AUTHOR: ANDREA CAVAGNINO (e-mail: andrea.cavagnino@polito.it)

ABSTRACT This paper presents the concept of efficiency mapping for large synchronous hydrogenerators, which are useful for evaluating hydropower generation performance *vis-à-vis* interconnected intermittent generation to machine efficiency-oriented design. Tests for loss segregation at rated conditions are needed, and models for loss variation along all operational areas are presented. The weighted average efficiency is obtained as the summation of all operating load point efficiencies times related weights, defined according to criteria or from a 2D-histogram of machine operation. The proposed methodology is applied and compared for two machine designs and to an existent machine under operation.

INDEX TERMS Hydrogenerator, modeling, efficiency, testing, losses.

NOMENCLATURE

A_k	Weighting factor
b_v	The slope of the air-gap line
b_i	Polynomial coefficients of the saturation curve
E_G	Induced EMF (pu)
E_P	Induced EMF behind the Potier reactance (pu)
n	Number of considered points
i	Dummy variable
I_A	Armature terminal current (A) or (pu)
I_F	Field current (A)
P_a	Armature winding current loss (kW)
P_b	Loss in the bearings (kW)
P_{br}	Brushes loss (kW)
P_c	Armature core loss (kW)
P_{ex}	Exciter loss (kW)
P_f	Field winding current loss (kW)
P_s	Stray load loss (kW)
P_{wf}	Windage and friction loss (kW)
P	Dispatched active power (kW) or (pu)
Q	Dispatched reactive power (kvar) or (pu)
R_A	Armature resistance (pu)
U_A	Armature terminal voltage (V) or (pu)
X_d	Direct axis synchronous reactance (pu)

X_q	Quadrature axis synchronous reactance (pu)
X_P	Potier reactance (pu)
δ	Loading angle (rad)
φ	Load angle (rad)
η	Efficiency (pu) or (%)
η_A	Average efficiency (pu) or (%)
η_w	Weighted average efficiency (pu) or (%)

I. INTRODUCTION

The Future application of hydrogenerators involves the complementary operation with intermittent renewable power generation. Energy storage systems have been proposed to solve new renewables' intermittence [1]–[3]. However, in cases where storage is not available, the threat caused by the generation intermittency and voltage regulation are usually rendered to hydropower plants.

Therefore, for PV and wind generation, in moments of high irradiance or high wind speeds, the renewable generation is high, and hydrogenerators are set to a minimum generation. The reciprocal is also true, resulting in considerable active power variation over time [4], [5]. For instance, Fig. 1 shows the net load evolution on a typical spring day in California; the
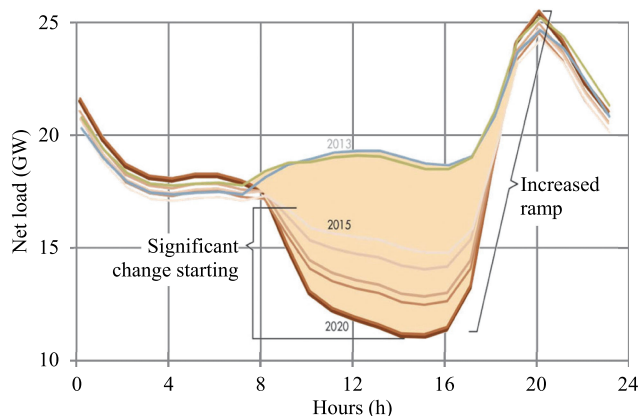
FIGURE 1. The "Duck Curve" shows the net load variation in areas with high solar generation penetration [13].
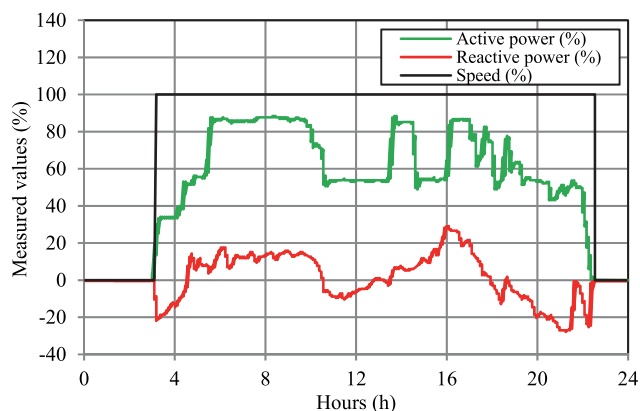

FIGURE 2. The active and reactive power of a typical indirectly cooled generator in the 300 MVA class is connected to a grid and a flexible load [14]. In this picture, 100% speed refers to the machine under operation.

steepest ramp of a necessary additional generation of about 4 GW/h can be seen [6].

Reactive power has also been widely dispatched, forcing the hydrogenerators to work virtually as a synchronous condenser, dewatered or not, as long as new renewables cannot handle extent voltage regulations, lending this effort to the installed synchronous generators, as shown in Fig. 2 [7].

The variability of the generation brings additional limiting issues. As a function of the loading changes, the temperature variation results in expansion and contraction of the insulation material, creating cracking, voids, and the increase of partial discharge activities, causing generator aging and lifetime reduction [8], [9].

Starts and stops may result in insufficient oil lubrication and friction increase between bearings and shaft [10], [11]. Additionally, forbidden operating areas, vibration, and cavitation are dictated from the hydro turbine side, limiting the operating range of the hydrogenerator beyond its capability curve [12], [13]. Such operational limits of mechanical order are not covered in this paper.

In the past, hydrogenerators used to work close to rated conditions of power, power factor, and efficiency. But nowadays, due to either renewable generation or independent system operator requirements, the loading of a generator can undergo profound variations throughout the day, with direct influence on the losses and in the operating efficiency [14].

The losses of any electrical machines are of diverse nature [15], namely: stator and rotor current losses [16], [17], iron loss [18], [19], stray-load loss [20], [21], and windage loss [22], [23]. Excitation loss, brush loss, and bearings loss are taken into account when necessary. Many factors influence these losses; some of these losses are constant with current, and others may vary either with the stator current or with the rotor current. In short, for constant speed and voltage generators, the total losses vary with the loading of the machine [15].

This work contributes to determining the weighted average efficiency (WAE), a single number that considers all the operating conditions rather than a single number reflecting only the rated condition. The WAE calculation includes its theoretical basis, loss modeling, and weights definition based on experience or a 2D-histogram.

This manuscript is divided into sections, Section I being this introduction. Section II presents practical segregation of losses, and Section III shows models for the diverse losses that are in synchronous generators. Section IV discusses the WAE concept and calculation.

Two types of examples are explored in this paper. The first type refers to brand-new generators, and it is addressed in Section V, where the efficiency results are compared to manufacturer expectations. Section VI presents the second example with the calculation of the WAE of an existing generator. Section VII and Section VIII bring the discussion and the main conclusions, respectively.

II. LOSSES SEGREGATION

The diverse type of losses can be determined using several ways [24], [25]. The most practical method for testing large generators is the thermodynamic method [26]. The loss segregation is achieved by performing tests with the generator at different conditions. The operating conditions, often called *running*, may be divided into first, second, and third running, described below.

A. FIRST RUNNING

In the first running, the machine is rotated by the turbine at the rated speed, with no currents in the stator and field windings. After reaching thermal equilibrium, the thermodynamic method is applied to measure the losses. The measured losses comprise only the windage and friction losses. The so-called no-load loss summarizes the power dissipated in the cooling system and radiation and convection in the surfaces, i.e., covering concrete walls and shaft.

B. SECOND RUNNING

The machine is run at no-load, rated speed, with excitation to obtain rated voltage in the terminals. In this condition, there
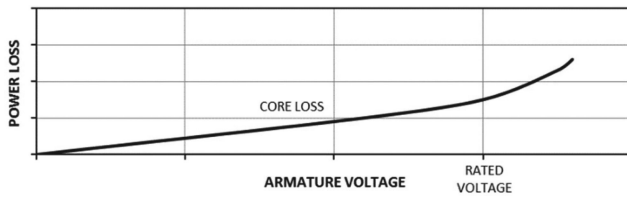
FIGURE 3. Armature core loss dependence with the applied voltage, as described in the IEEE STD 115 [16].

FIGURE 4. Armature resistance loss (short-circuit loss) and stray-load loss dependence with the square of armature current, as described in the IEEE STD 115 [16].

are only no-load losses, core losses, and field copper losses. The core loss plus the loss in the field copper is the subtraction of the loss obtained in the first running from the losses obtained in the second running results. The field resistance loss can be determined from the product of excitation voltage and excitation current. Therefore, the core loss in no-load conditions can be obtained.

C. THIRD RUNNING

The third running is conducted with the machine under a permanent three-phase short-circuit and sufficiently excited to achieve rated armature current. During this test, the machine is subject to stray-load loss and armature copper loss.

The stray-load loss is determined by subtracting the armature copper loss, field copper loss, and no-load loss from this test's total loss.

The armature copper loss is determined from the measured resistance corrected with temperature, and this test's armature current. Field loss is determined as the product of the excitation current and voltage, and the no-load loss is obtained in the first running, with eventual correction due to the air density and pressure variations.

III. LOSSES MODELING

For a grid-connected hydrogenerator, some types of losses can be considered constant; nevertheless, other types of losses may be modeled as a function of either terminal current or field current. Those characteristics are detailed as follows.

A. CURRENT INDEPENDENT LOSSES

The constant losses are those that do not vary with loading. In a synchronous generator, they are the windage and friction loss and the armature core loss. The windage loss is proportional to the speed raised to the third power. Thus, it is considered constant since a generator in a hydropower plant works at a nearly constant speed to achieve the system's frequency. There is a relatively small variation of friction loss with the loading of the machine. However, a hydro machine's significant effort is the turbine axial force, which is almost constant.

The armature core loss is a function of the frequency and the applied voltage. While frequency suffers tiny variation, the voltage may vary in a short-range established by grid codes. The IEEE STD 115 presents the core losses as a function of the terminal voltage, as shown in Fig. 3.
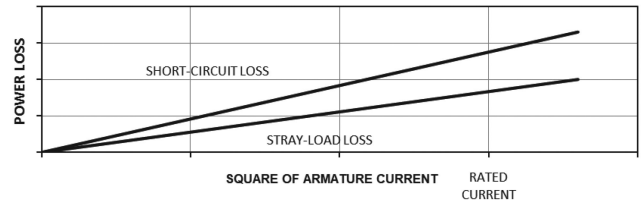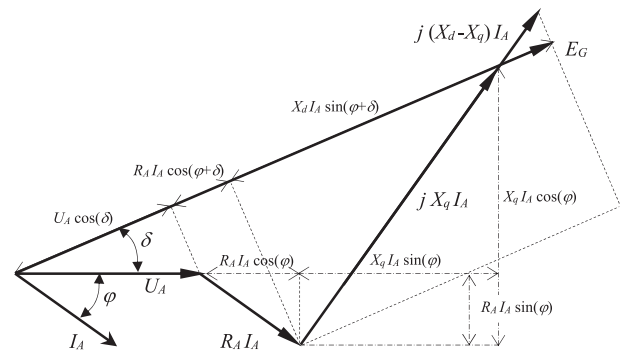

FIGURE 5. Phasor diagram of a generator connected to an inductive load is used to calculate induced EMF [27].

Therefore, the summation of windage, friction, bearings, and armature core losses is a current independent loss and is considered constant with the loading.

B. ARMATURE CURRENT DEPENDENT LOSSES

The armature current dependent losses are the armature winding copper loss and the stray-load loss. Both of them varies with the square of the armature current as depicted in Fig. 4. (1) may be used to obtain the armature terminal current as a function of the dispatched active and reactive powers and terminal armature voltage.

$$I_A = \frac{\sqrt{P^2 + Q^2}}{\sqrt{3}\, U_A} \qquad (1)$$

C. FIELD CURRENT DEPENDENT LOSSES

Field current dependent losses are the field winding copper loss, the voltage drop in the brushes, and exciter loss. The first two losses vary with the field current's square, whereas the third loss is proportional to the field current.

The field current can be calculated using a well-known formulation, such as that presented in [24], which depends on the direct and quadrature synchronous reactances, the Potier reactance, and the armature resistance. Considering the phasor diagram of Fig. 5, yields.

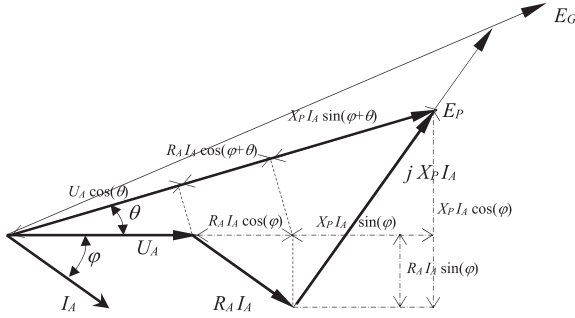$$\varphi = \arctan\left(Q/P\right) \qquad (2)$$

FIGURE 6. Phasor diagram of a generator connected to an inductive load used to calculate excitation quantities [27].

$$\delta = \arctan \left[\frac{X_q \, I_A \cos(\varphi) - R_A \, I_A \sin(\varphi)}{U_A + R_A \, I_A \cos(\varphi) + X_q \, I_A \sin(\varphi)} \right] \quad (3)$$

The Induced EMF is:

$$E_G = U_A \cos(\delta) + R_A \, I_A \cos(\varphi + \delta) + X_d \, I_A \sin(\varphi + \delta) \quad (4)$$

Referring to the phasor diagram of Fig. 6, the angle of the voltage behind Potier reactance is [27]:

$$\theta = \arctan \left[\frac{X_P \, I_A \cos(\varphi) - R_A \, I_A \sin(\varphi)}{U_A + R_A \, I_A \cos(\varphi) + X_P \, I_A \sin(\varphi)} \right] \quad (5)$$

And its value is:

$$E_P = U_A \cos(\theta) + R_A \, I_A \cos(\varphi + \theta) + X_P \, I_A \sin(\varphi + \theta) \quad (6)$$

The field current for any loading condition is the current necessary to obtain E_G in the no-load saturation curve, plus the saturation increment. The saturation increment is the difference between the excitation current value required to induce E_P on the air-gap line and value of field current corresponding to E_P on the no-load saturation curve.

Considering the non-linear part of the no-load saturation curve as an *n*-th order polynomial with b_i coefficients, the field current can eventually be computed as in (7). For per unit values, the slope of the air-gap line (b_v) is one, [28].

$$I_F = \frac{E_G}{b_v} + \left(\sum_{i=1}^{n} b_i \, E_P^i \right) - \frac{E_P}{b_v} \quad (7)$$

D. LOSSES AND EFFICIENCY CALCULATION AT ANY LOADINGS

Considering armature current dependent losses and field current dependent losses, the following simple models can be applied to determine the losses at any loading.

$$P_a = P_a^* \left(\frac{I_A}{I_A^*} \right)^2 \quad (8)$$

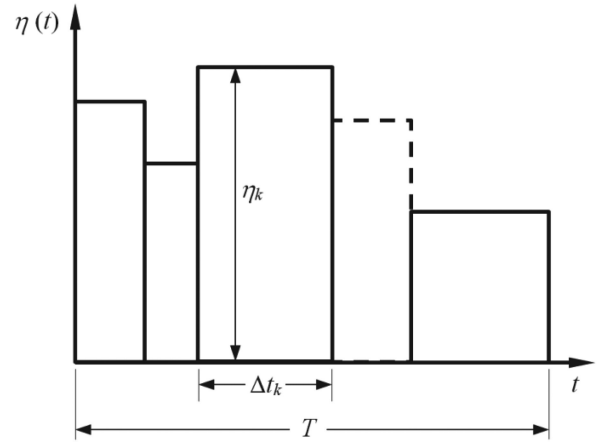$$P_f = P_f^* \left(\frac{I_F}{I_F^*} \right)^2 \quad (9)$$

FIGURE 7. time-depending efficiency trend for WAE computation.

$$P_s = P_s^* \left(\frac{I_A}{I_A^*} \right)^2 \quad (10)$$

$$P_{br} = P_{br}^* \left(\frac{I_F}{I_F^*} \right)^2 \quad (11)$$

$$P_{ex} = P_{ex}^* \left(\frac{I_F}{I_F^*} \right) \quad (12)$$

$$P_c = P_c^* \left(\frac{U_A}{U_A^*} \right)^2 \quad (13)$$

The variables denoted with ∗ refers to quantities and losses measured in rated conditions. I_A and I_F are calculated for any loading conditions using (1) and (7). The exciter loss is not current squared because it is not a resistance loss type. It depends on the power supplied to the machine excitation winding and the exciter's nature, i.e., rotating type or static type. In this work, the exciter loss is modeled as a linear function of the excitation current.

As long as the windage and given area friction, bearings, and core losses are considered constant, the efficiency at any loading can be obtained (14).

$$\eta = \frac{P}{P + P_a + P_f + P_s + P_{br} + P_{ex} + P_b + P_{wf} + P_c} \quad (14)$$

IV. WEIGHTED AVERAGE EFFICIENCY

It was realized that a generator operates at several loadings rather than only in the rated condition and, therefore, the knowledge of the energy conversion at those loading points is critical, just the knowledge of efficiency at the rated condition is. As the power, losses, and efficiency vary over time, as shown in Fig. 7 for efficiency, the average efficiency can be calculated as:

$$\eta_A = \frac{1}{T} \int_0^T \eta(t) \, dt \quad (15)$$

TABLE 1. Rated Quantities

Quantity	Unit	M#1	M#2
Rated apparent power	MVA	82.25	679
Power factor	-	0.9	0.9
Rated voltage	kV	13.8	18
Rated current	A	3441	21779
Rated speed	rpm	100	85.7
Runaway speed	rpm	300	162
Rated frequency	Hz	60	60
Direct axis reactance (X_d)	pu	1.09	0.98
Quadrature axis reactance (X_q)	pu	0.72	0.69
Potier reactance (X_P)	pu	0.2	0.18

TABLE 2. Full Load Losses and Efficiency

Quantity	Unit	M#1	M#2
Core loss	kW	240.4	1577.8
Brush loss	kW	2.5	6.5
Bearing loss	kW	0	60
Windage and friction loss	kW	200.0	2781
Armature winding current loss	kW	425.2	1570.8
Field winding current loss	kW	286.1	1467
Excitation loss	kW	23.1	117.9
Stray-load loss	kW	144.6	830.9
Efficiency	%	98.42	98.78

The WAE is obtained as the summation, for diverse loading points, of the observed efficiency multiplied by a weight. The weights are established from the experience or the importance grant to given loading for brand-new generators. For existent generators, each load's weight is calculated as the probability of occurrence for that given load, as in (16).

$$A_k = \frac{\Delta t_k}{T} \qquad (16)$$

Therefore, the WAE is calculated according to (17).

$$\eta_w = \sum_{k=1}^{n} A_k \, \eta_k \qquad (17)$$

Given that

$$\sum_{k=1}^{n} A_k = 1 \qquad (18)$$

Where η_w is the weighted average efficiency, n is the number of considered loading points. A_k and η_k are, respectively, the weighting factor and the efficiency corresponding to each loading point.

The WAE was formally suggested in [14]. New versions of recognized standards, as IEC 60034-33 and IEEE C50.12, are already considering implementing this concept in their revisions [29], [30].

The analysis departs from constructing the efficiency map in the P-Q plane. It means that for each P-Q pair, the efficiency is determined using the models presented in Section III. The capability chart is drawn to recognize the generator limits of operation. Additionally, it is set-up a 2D-histogram for existing machines from the generator's loading within a period of interest. The 2D-histogram is also drawn in the P-Q plane, and the capability chart limits it. The WAE is obtained by crossing the efficiency map with the 2D-histogram, i.e., the summation of point-by-point multiplication of the efficiency map with the 2D-histogram results in the sought WAE.

V. COMPARISON TO DESIGN DATA

The proposed methodology was verified by comparing its results with information received from a manufacturer. Two large hydrogenerators were evaluated. Table 1 presents rated quantities, and the design losses are depicted in Table 2, along
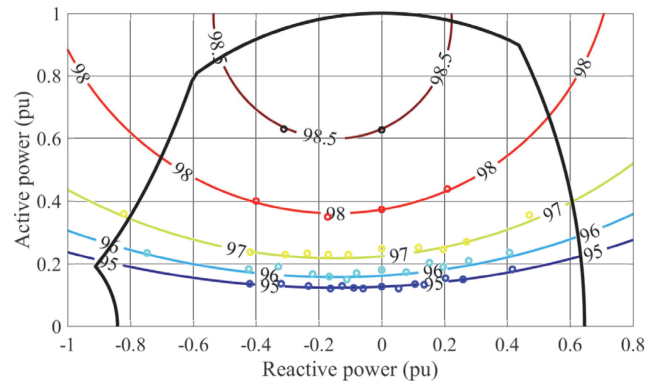

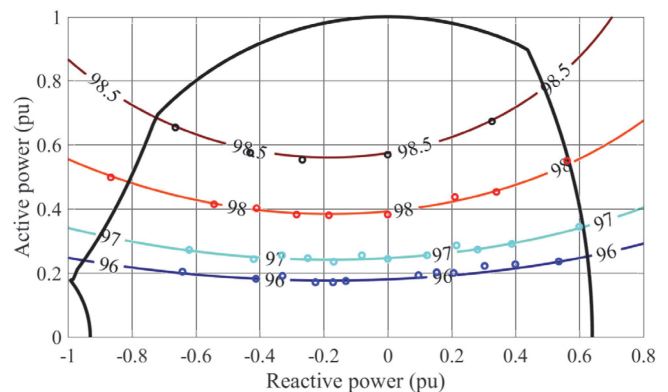**FIGURE 8.** Efficiency map for the 82.25 MVA, M#1 machine.

FIGURE 9. Efficiency map for the 679 MVA, M#2 machine.

with their rated efficiency. The first machine is a Bulb generator, while a Francis turbine drives the second.

The efficiency map of machines M#1 and M#2 are depicted in Fig. 8 and Fig. 9, respectively. The lines represent the calculated iso-efficiency curves, while the dots are efficiencies obtained from the machine proven design software. The agreement between the calculated lines and the given design values demonstrates the suitability of the proposed methodology.

WAE for these two machines was calculated using the weighting factors and loads of Table 3. The weights and reference loads are defined upon the purchaser and manufacturer's agreement, considering the expected operation regime.

TABLE 3. Adopted Weights for Given Generator Loading and Efficiency

P (pu)	0.2	0.4	0.6	0.8	0.8	0.8	0.8	0.8
Q (pu)	0	0	0	0	-0.4	-0.2	0.2	0.4
A_i	0.05	0.20	0.30	0.20	0.05	0.10	0.05	0.05
$\eta_{\#1}$ (%)	96.70	98.10	98.47	98.59	98.55	98.61	98.49	98.53
$\eta_{\#2}$ (%)	96.37	98.03	98.54	98.76	98.75	98.78	98.70	98.59
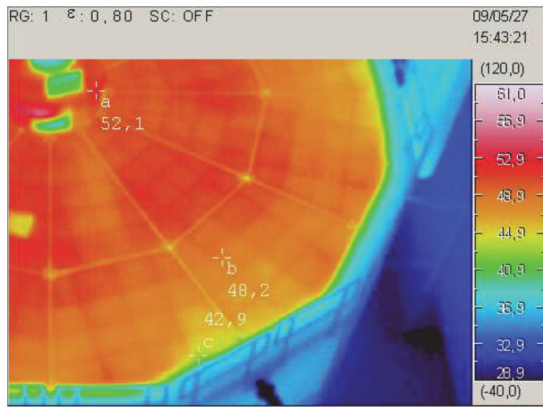
FIGURE 10. Furnas hydropower plant's unit #6 under an efficiency test.

TABLE 4. Rated Information

Power	MVA	160
Power factor	-	0.95
Voltage	kV	15
Speed	r/min	150

The calculated WAE for the first and second machines are, respectively, 98.35% and 98.41%, while the rated efficiency values, as depicted in Table 2, are 98.42% and 98.78%, respectively.

The efficiency map reveals that the maximum efficiency is not in the rated point but with a lower excitation current. Reduction of the excitation current implies reducing the armature current until a certain point when it starts increasing. The minimum summation of field and armature current losses leads to maximum efficiency, defining the efficiency map aspect. Bulb generators have distinct design metrics [31], resulting in a particular efficiency map shape. This point raises the possibility of the efficiency-oriented design to attend a given load behavior with maximum efficiencies.

VI. A CASE STUDY WITH EXPERIMENTAL RESULTS

The proposed methodology was applied to generator #6 of Furnas hydropower plant, as shown in Fig. 10. The generator is coupled to a Francis turbine, and its primary rated data are given in Table 4. Tests were performed in this generator to obtain its efficiency and loss segregation close to rated loading. The no-load saturation curve was determined to model the field current. The efficiency map was calculated using the proposed technique, and a 2D-histogram was obtained from its annual operation. Infrared thermodynamic measurements were applied to conduct the tests [26].

TABLE 5. Losses Measured in the First Running

Loss in the covering surface	kW	18.74
Loss in the walls	kW	4.15
Loss in the covering of the turbine	kW	3.90
Loss in the radiators	kW	683.68

TABLE 6. Losses Measured in the Second Running

Loss in the covering surface	kW	24.02
Loss in the walls	kW	9.76
Loss in the covering of the turbine	kW	10.82
Loss in the radiators	kW	1388.26

TABLE 7. Losses Measured in the Third Running

Loss in the covering surface	kW	23.75
Loss in the walls	kW	8.85
Loss in the covering of the turbine	kW	10.46
Loss in the radiators	kW	1379.35

TABLE 8. Ambient Quantities

Atmospheric pressure	mbar	936.67
Relative humidity	%	34.33
Temperature	°C	37.8
Air density	kg/m³	1.134

TABLE 9. Full Load Losses and Efficiency

Windage and friction loss	kW	710.47
Core loss	kW	539.87
Stator copper loss	kW	327.05
Stray-load loss	kW	237.07
Rotor copper loss	kW	477.81
Brush losses	kW	5.93
Excitation loss	kW	33.96
Bearing loss	kW	156.17
Power output	kW	154608
Efficiency	%	98.41%

A. TESTS FOR LOSSES SEGREGATION

As described, three runnings are necessary to obtain efficiency and losses. The main losses measured in the first running are depicted in Table 5. The total loss is the summation of the losses in the radiator and the radiant surfaces and represents the windage and friction, which eventually is 710.47 kW.

The main measurements in the second running are presented in Table 6. The rotor current loss is measured in the rings of the machine resulting in 182.52 kW. Therefore, the core loss is 539.87 kW.

The total losses measured in the third running are presented in Table 7. The stator and rotor current loss are, respectively, 355.93 kW and 85.94 kW; therefore, the stray-load loss is 270.07 kW. The ambient conditions during the tests are shown in Table 8. The losses and efficiency were obtained for output of 154.6 MW, close to rated conditions, as described in Table 9.

B. NO-LOAD SATURATION TEST

The no-load saturation test was applied to the machine under study, obtaining several pairs of field current and induced

TABLE 10. Polynomial Coefficients to Represent Saturated Part of the No-Load Curve

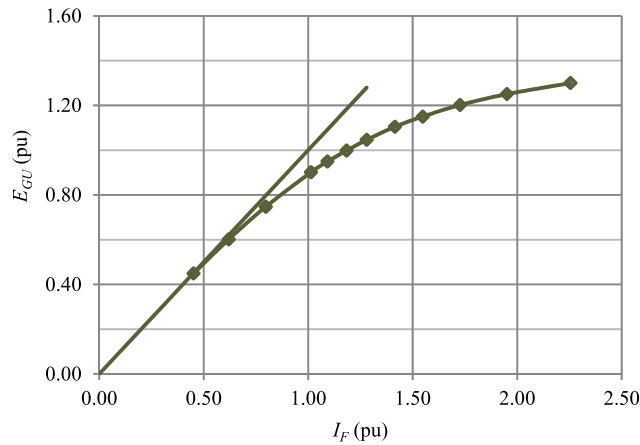| Coefficient	b_0	b_1	b_2	b_3	b_4
Value	2.0737	-10.959	24.850	-22.228	7.4417

FIGURE 11. No-load saturation curve with the air-gap line and polynomial representation of its saturated part.
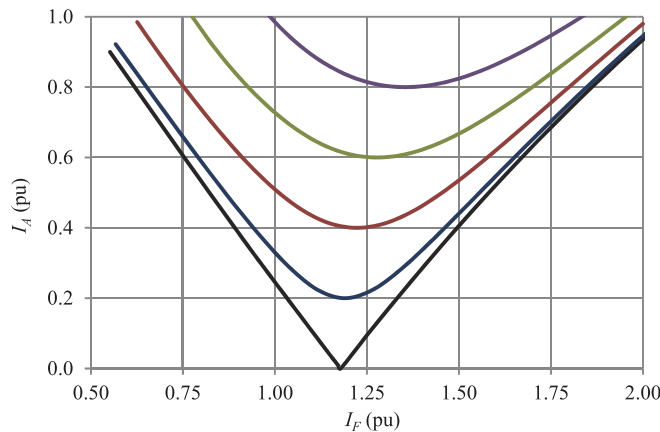

FIGURE 12. Mordey diagram, or V-Curve family, for the machine under study.

EMF measurements. The obtained data were analyzed using the same methodology presented in [19]. The air-gap line slope is 14.61 V/A, and the rated field current to achieve rated voltage in the air gap is 592.7 A.

A fourth-order polynomial regression over the per-unit saturated part of the no-load curve resulted in the coefficients presented in Table 10. The complete per-unit saturation curve is shown in Fig. 11.

C. FIELD CURRENT FOR ANY LOAD

While the armature current is directly proportional to the complex power output, the field current must be calculated for each operating point considering saturation as previously described. For this generator X_d is 0.8 pu, X_q is 0.6 pu, X_P is 0.18 pu, and R_A is 0.00232 pu. Applying (1) to (7), the Mordey
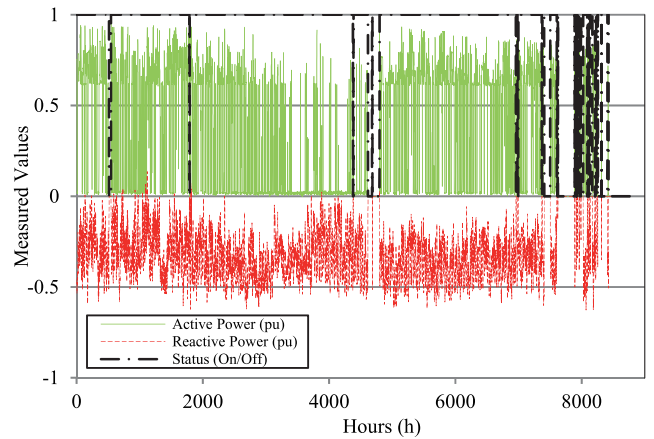

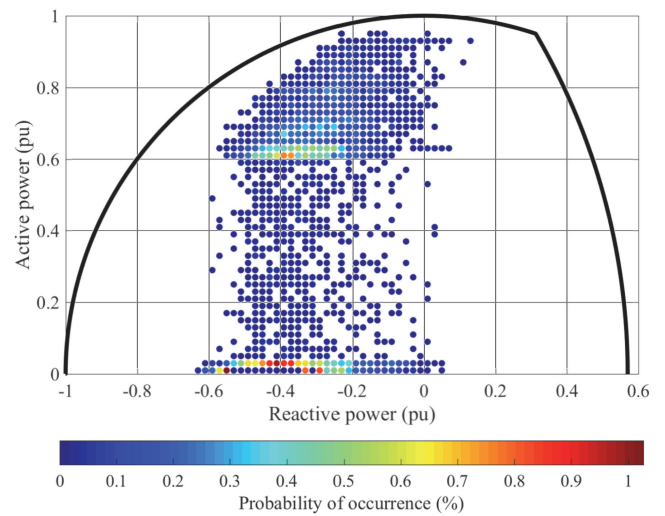**FIGURE 13.** Active and reactive powers demand during a given year.

FIGURE 14. 2D-histogram in the P-Q plane. The color bar is the time percentage of operation in each loading point inside the machine's capability chart.

diagram, or the V-curves family, is obtained, relating armature current to field current, for several constant active powers. Fig. 12 presents the Mordey diagram, for powers varying from 0 to 1 pu, in steps of 0.2 pu.

D. 2D-HISTOGRAM

The generator under study has particular characteristics of operation as long as it works at low active power for a part of the time; positive or negative reactive power is always demanded grid voltage regulation purposes. Fig. 13 shows measured values of active and reactive powers during an entire year; the operating status is also presented in this figure showing the intervals when the machine is turned on or off, depicting its random operative nature.

Fig. 14 presents the 2D-histogram in the P-Q plane and the probability of a given power pair in the year. This kind of operation is typical in areas new renewables generation is
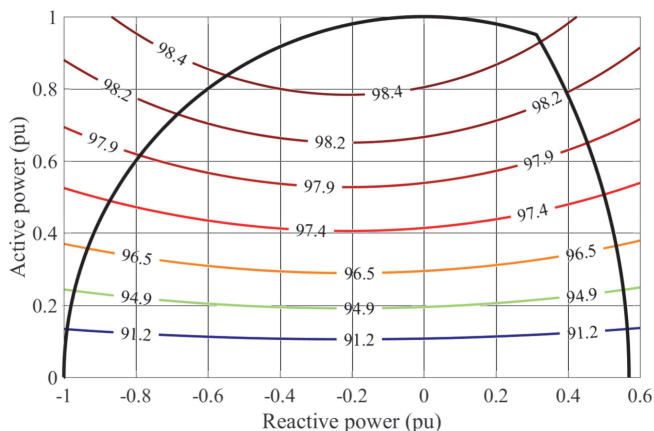
FIGURE 15. Efficiency map for the machine under study with "iso-efficiency" curves along with the capability chart of the machine.
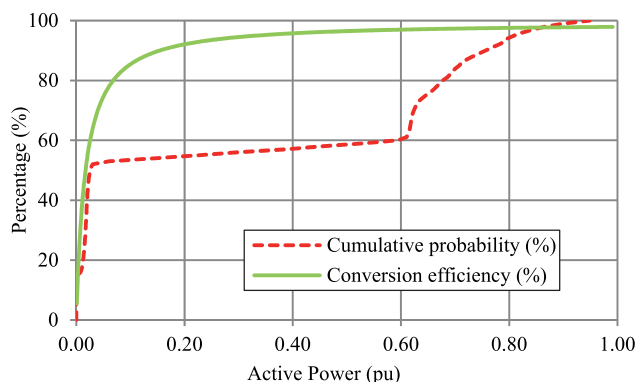

FIGURE 16. Cumulative probability and conversion efficiency for unitary power factor as function of active power for the considered machine.

on the increase, of intermittent power generation and voltage control.

E. EFFICIENCY MAPPING

The loss for every loading is determined using the models presented in Section III. The application of those formulas requires the knowledge of losses at rated conditions, armature current, and field current. All of those components are now known, and the machine's efficiency mapping under study can be determined. Fig. 15 shows the tested machine's efficiency map, presenting the iso-efficiency curves limited by its capability chart.

For better readability, efficiencies lower than 91.2% were not shown in Fig. 14. It is important to remark that in the omitted region (i.e., for lower active powers), the efficiency variation is very steep, and the figure would contain several lines because it is a region with a substantial variation in the efficiencies, as can be seen in Fig. 16.

F. WEIGHTED AVERAGE EFFICIENCY

Under (17), the WAE is the summation, for all the possible operative loading points, of weight times the generator's

efficiency. In the considered application, the weight is the percentage of time the machine operates at a given load, i.e., their probability of occurrence. Assuming the obtained efficiency map and the histogram of this generator's operation, the calculated WAE is 64.84%.

The low value of WAE found in this particular application arises due to the subsequent periods this machine operates at low active power generation at low energy conversion efficiency. Fig. 16 presents the cumulative probability and the conversion efficiency as a function of active power. One can observe that about 40% of the time, the active power is higher than 60%, with efficiencies greater than 97%; on the other hand. Also, about 50% of the time, active power is below 2%, with efficiencies lower than 55%.

It must be recognized that those values are weighted by their probabilities of occurrence, resulting in a considerable reduction of the WAE concerning the rated efficiency. If a low limit of active power generation of 60% is adopted, the WAE result in 98.01%, which approximates the rated efficiency of 98.41%. This fact reinforces the importance of evaluating the WAE rather than considering a single and rated efficiency value.

VII. DISCUSSION

The presented computation scheme is suitable for calculating the efficiency in diverse loading conditions, resulting in the WAE. Simple equations based on theory and proven standards are used for this purpose. This point is vital because the variations of active and reactive powers of 0.01 per unit are typically considered, which would result in more than 20000 simulations, which is accomplished in a couple of seconds. The computational time required for this significant number of simulations would not be practical if more complex modeling, for instance, the finite element method, were used.

This procedure is necessary because, with renewable generation penetration, the synchronous generators do not work anymore in a single rated load but, on the opposite, operate in variable conditions as a function of the dispatch of new renewables connected to the system. This fact would bring additional economic costs because the manufacturer should present high-efficiency equipment in the rated condition and the several expected loading for a new generator. Besides, insulation must be conceived considering this new regime of loading changing.

The described challenges resulting from the intermittent generation from new renewables can be solved using energy storage systems; however, their influence in the WAE could be reduced by establishing a low limit for active power generation in regular synchronous generators.

It is important to remark that those issues are critical points in a renewable generation scenario, accounting for power sources with considerable variability. Therefore, aiming at harmonization, new revisions of standards IEC 60034-33 and IEEE C50.12, may include the concept of WAE, a proposal of reference loads and weighting factors, and different duty-cycles in addition to the existing ones.

Finally, it should be noted that variable speed hydro generation actually under investigation to improve the WAE, as the so-called constant losses could be reduced [32]. Furthermore, a crucial aspect is that the WAE can be used for the efficiency-oriented design of the hydrogenerators. As long as the efficiency map's shape follows the percentage losses distribution, the machine can be optimally designed to attend to a particular loading cycle or expected operation.

VIII. CONCLUSION

This paper presented a methodology to obtain the efficiency map and the computation of the WAE. The proposed procedure starts from the conventional theory and is reported step-by-step to allow engineers and practitioners to replicate the findings. The proposed approach is verified using both design and measured data by considering two brand new generators and an actual hydrogenerator operated under an impacting duty-cycle imposed by renewables in the grid. In the second case, a very impressive loss of efficiency is proved. The procedure applicability and the obtained findings are critically discussed, and the potential use of the weighted average efficiency concept for future developments, including the efficiency-oriented design of machines.

ACKNOWLEDGMENT

REFERENCES

[1] J. P. Barton and D. G. Infield, "Energy storage and its use with intermittent renewable energy," *IEEE Trans. Ener. Convers*, vol. 19, no. 2, pp. 441–448, Jun. 2004.
[2] A. Mamen and U. Supatti, "A survey of hybrid energy storage systems applied for intermittent renewable energy systems," in *Proc. 14th ECTI-CON*, Phuket, Thailand, 2017, pp. 729–732.
[3] P. A. V. Vieira, E. C. Bortoni, and A. S. Bretas, "A new approach of conti-varlet method applied to a PV system to size a battery energy storage," in *Proc. IEEE Power Tech. Conf.*, Milan, Italy, 2019, pp. 1–5.
[4] V. Gevorgian, Y. Zhang, and E. Ela, "Investigating the impacts of wind generation participation in interconnection frequency response," *IEEE Trans. Sustain, Energy*, vol. 6, no. 3, pp. 1004–1012, Jul. 2015.
[5] J. J. Roberts, A. M. Cassula, J. L. Silveira, E. C. Bortoni, and A. Z. Mendiburud, "Robust multi-objective optimization of a renewable based hybrid power system," *Appl. Energy*, vol. 223, pp. 52–68, 2018.
[6] P. Denholm, M. O'Connell, G. Brinkman, and J. Jorgenson, "Overgeneration from solar energy in california: A field guide to the duck chart," NREL, Golden, CO, NREL/TP-6A20-65023, 2015.
[7] A. Joswig, H. Steins, and J. R. Weidner, "Impact of new flexible load operation and grid codes on turbine generators with a focus on end windings," in *Proc. Power Gen. Europe*, Amsterdam, the Netherlands, 2015, pp. 1–25.
[8] I. Kremza, S. Bomben, T. Black, and A. Shaikh, "Qualification test results on multi-turn coils of large hydrogenerators," in *Proc. IEEE Elect. Insul. Conf.*, Philadelphia, PA, USA, 2014, pp. 434–439.
[9] A. Griffo, I. Tsyokhla, and J. Wang, "Lifetime machines undergoing thermal cycling stress," in *Proc. IEEE Energy Convers. Congr. Expo.*, Baltimore, MD, USA, USA, 2019, pp. 3831–3836.
[10] R. Gawarkiewicz and M. Wasilczuk, "Wear measurements of self-lubricating bearing materials in small oscillatory movement," *Wear*, vol. 263, pp. 458–462, 2007.
[11] D. Momcilovic, Z. Odanovic, R. Mitrovic, I. Atanasovska, and T. Vuherer, "Failure analysis of hydraulic turbine shaft," *Eng. Fail. Anal.*, vol. 20, pp. 54–66, 2012.
[12] W. Yang et al., "Burden on hydropower units for short-term balancing of renewable power systems," *Nat. Commun.*, vol. 9, 2018, Art. no. 2633.
[13] E. Doujak, "Effects of increased solar and wind energy on hydro plant operation," *Hydro Rev. Worldwide*, vol. 22, no. 6, pp. 28–31, 2014.
[14] Electrical Machinery Committee Task Force on Grid Code Impacts on Generator Standards, "Consequences of diverse grid code requirements on synchronous machine design and standards," *IEEE PES, Tech. Rep.* PES-TR69, Nov. 2018.
[15] J. Pyrhonen, T. Jokinen, and V. Hrabovcova, "Losses and heat transfer," in *Design of Rotating Electrical Machines*. New York, NY, USA: Wiley, 2013, pp. 523–569.
[16] Y. Zhao, D. Li, T. Pei, and R. Qu, "Overview of the rectangular wire windings AC electrical machine," *CES Trans. Elect. Mach. Syst.*, vol. 3, no. 2, pp. 160–169, Jun. 2019.
[17] M. Fujita, Y. Kabata, T. Tokumasu, K. Nagakura, M. Kakiuchi, and S. Nagano, "Circulating currents in stator coils of large turbine generators and loss reduction," *IEEE Trans. Ind. App.*, vol. 45, no. 2, pp. 685–693, Mar./Apr. 2009.
[18] A. Fatemi, D. M. Ionel, N. A. O. Demerdash, D. A. Staton, R. Wrobel, and Y. C. Chong, "Computationally efficient strand eddy current loss calculation in electric machines," *IEEE Trans. Ind. App.*, vol. 55, no. 4, pp. 3479–2489, Jul./Aug. 2019.
[19] M. Ranlöf, A. Wolfbrandt, J. Lidenholm, and U. Lundi, "Core loss prediction in large hydropower generators: Influence of rotational fields," *IEEE Trans. Mag.*, vol. 45, no. 8, pp. 3200–3206, Aug. 2009.
[20] M. P. Calasan, D. S. Petrovic, and M. M. Ostojic, "Electrical braking of synchronous generators for combined generator and water turbine bearings as well as stray-load losses determination," *IET Elect. Power App.*, vol. 7, no. 4, pp. 313–320, 2013.
[21] H. C. Karmaker, "Stray losses in large synchronous machines," *IEEE Trans. Ener. Convers*, vol. 7, no. 1, pp. 148–153, Mar. 1992.
[22] L. Weili, H. Jichao, Z. Xingfu, and L. Yong, "Calculation of ventilation cooling, three-dimensional electromagnetic fields, and temperature fields of the end region in a large water–hydrogen–hydrogen-cooled turbogenerator," *IEEE Trans. Ind. Elect.*, vol. 60, no. 8, pp. 3007–3015, Aug. 2013.
[23] W. Li, D. Li, J. Li, and X. Zhang, "Influence of rotor radial ventilation ducts number on temperature distribution of rotor excitation winding and fluid flow state between two poles of a fully air-cooled hydrogenerator," *IEEE Trans. Ind. Elect.*, vol. 64, no. 5, pp. 3767–3775, May 2017.
[24] *IEEE Guide for Test Procedures for Synchronous Machines Including Acceptance and Performance Testing and Parameter Determination for Dynamic Analysis*. IEEE Standard 115, 2019.
[25] *Rotating electrical machines - Part 4: Methods for determining synchronous machine quantities from tests*. IEC 60034-4, Geneve, 2018.
[26] E. C. Bortoni, R. T. Siniscalchi, and J. A. Jardini, "Determination of hydrogenerator efficiency using infrared thermal imaging techniques," *IEEE Trans. Energy Convers.*, vol. 26, no. 4, pp. 1134–1139, Dec. 2011.
[27] B. T. Araujo, M. S. Han, B. Kawkabani, and E. C. Bortoni, "Estimation of the armature leakage reactance using the constant excitation test," in *Proc. 22nd Int. Conf. Elect. Mach.*, 2016, Lausanne, Switzerland.
[28] E. C. Bortoni, P. V. V. da Silva, G. A. Braulio, and R. T. Siniscalchi, "Geometric characteristics of saturation tests in synchronous machines" in *Proc. IEEE PES Gen. Meeting*, Atlanta, GA, 2019, pp. 1–4.
[29] *Rotating Electrical Machines - Part 33: Specific Technical Requirements for Synchronous Hydrogenerators Including Motor-Generators*. IEC Standard IEC 60034-33, Genève, 2019.
[30] *IEEE Standard for 50 Hz and 60 Hz Synchronous Generators and Generator/Motors Coupled to Hydraulic Turbines and Rated 5 MVA and Above*, IEEE Standard C50.12, 2019.
[31] F. J. Garcia, M. K. I. Uemori, J. J. R. Echeverria, and E. C. Bortoni, "Design requirements of generators applied to low-head hydro power plants," *IEEE Trans. Energy Convers.*, vol. 30, no. 4, pp. 1630–1638, Dec. 2015.
[32] E. C. Bortoni et al., "The benefits of variable speed operation in hydropower plants driven by francis turbines," *Energies*, vol. 12, no. 19, 2019, Art. no. 3719.

EDSON DA COSTA BORTONI (Senior Member, IEEE) was born in Maringá, Brazil, in 1966. He received the electrical engineering degree from the Federal University of Itajubá (UNIFEI), Itajubá, Brazil, in 1990, the M.Sc. degree in energy systems planning from the University of Campinas, Campinas, Brazil, in 1993, the D.Sc. degree in power systems from the Polytechnic School of the University of São Paulo (USP), São Paulo, Brazil, in 1998, and the Habilitation from USP in 2012. He is a Full Professor with UNIFEI. He was a Visiting Scholar with the École Polytechnique Fédérale de Lausanne, Switzerland, and with Politecnico di Torino, Italy. His research interests include electrical machines design, testing, modeling, power generation, energy systems, sensors, and smart grids. He is a Subject Editor of the IET *Generation, Transmission & Distribution* journal, and an Assistant Editor of the *Flow Measurement and Instrumentation* journal. He is a Distinguished Lecturer of the IEEE Power and Energy Society (PES), a Member of the Electromagnetic Compatibility and Working Groups, Task Force, and the Chair of the Generator subcommittee and several technical sessions in conferences, including the PowerTech, the IEEE PES General Meeting, and the International Electric Machines & Drives (IEMDC). He is the Head of the Energy Efficiency Excellence Center, the President of the Brazilian Society of Energy Planning, and a Fellow Member of the International Hydropower Association and the International Society of Automation.

ROBERTO TEIXEIRA SINISCALCHI (Senior Member, IEEE) was born in Itajubá, Brazil, on January 24, 1967. He received the B.S. degree in electrical engineering in 1993, the M.Sc. degree in energy engineering in 2009 from Universidade Federal de Itajubá, Itajubá, Brazil, and the M.B.A. degree from Universidade Candido Mendes, Rio de Janeiro, Brazil. He is currently with the Minas Production Department of Furnas Centrais Elétricas, Ibiraci, Brazil . He is responsible for the operation and maintenance of three hydropower plants totaling 2872 MW, including the Furnas hydropower plant, ten power substations, and about 3000 km of transmission lines in 345 kV and 500 kV. He is a Member of the IEEE PES EMC, WG-4 (IEEE STD. C50.12), WG-7 (IEEE STD. 115), WG-8 (IEEE STD. C50.13), and WG-10 (IEEE STD. 1110). His research interest include maintenance, field testing, and power generation.

SILVIO VASCHETTO (Senior Member, IEEE) received the M.Sc. and Ph.D. degrees in electrical engineering from the Politecnico di Torino, Turin, Italy, in 2007 and 2011, respectively. He is currently an Assistant Professor with the Dipartimento Energia, Politecnico di Torino. He is involved in the analyses and electrical machine design for high-performance drive developments, aerospace, and automotive applications. He is a Member of the IEEE Industry Application Society and the Industrial Electronics Society. He is an Associate Editor for the IEEE TRANSACTIONS ON INDUSTRY APPLICATIONS and the IET *Electric Power Applications,* and a Reviewer for several transactions, journal, and international conferences of the scientific community.

MOSTAFA AHMADI DARMANI (Student Member, IEEE) was born in Tehran, Iran, in 1987. He received the M.Sc. degree in electrical engineering from Azad University, Tehran, Iran, in 2003. He is currently working toward the Ph.D. degree in electrical engineering with the Energy Department, Politecnico di Torino, Turin, Italy. From 2013 to 2018, he was an Electrical Engineer, a Consultant, and an Instructor with training centers and different industries in Iran. His main research interests include the design and analysis of electrical machines. He is a Member of the IEEE Industry Application Society and the Industrial Electronics Society. He is a Reviewer for several IEEE transactions and international conferences.

ANDREA CAVAGNINO (Fellow, IEEE) was born in Asti, Italy, in 1970. He received the M.Sc. and Ph.D. degrees in electrical engineering from the Politecnico di Torino, Turin, Italy, in 1995 and 2000, respectively. He is a Full Professor with the Politecnico di Torino. He has authored or coauthored more than 200 papers. His research interests include electromagnetic design, thermal design, and the energetic behavior of electrical machines. He was the recipient of the four best paper awards. He cooperates with factories for a direct technological transfer, and he has been involved in several public and private research projects. He is an Associate Editor for the IEEE TRANSACTIONS ON ENERGY CONVERSION, the Past Chair of the Electrical Machines Technical Committee of the IEEE Industrial Electronics Society, and a Past Associate Editor for the IEEE TRANSACTIONS ON INDUSTRIAL ELECTRONICS and the IEEE TRANSACTIONS ON INDUSTRY APPLICATIONS. He was a Guest Editor of six Special Sections for the IEEE TRANSACTIONS ON INDUSTRIAL ELECTRONICS. He was the Technical Program Chair of the IEEE-IEMDC 2015 conference. He is a Reviewer for several IEEE transactions, other international journals, and conferences.